ELSEVIER

Computer Methods and Programs in Biomedicine 68 (2002) 1–14

Computer Methods and Programs in Biomedicine

www.elsevier.com/locate/cmpb

Generalized linear least squares algorithms for modeling glucose metabolism in the human brain with corrections for vascular effects

Weidong Cai [a,b], Dagan Feng [a,b,*], Roger Fulton [a,c], Wan-Chi Siu [b]

[a] *Basser Department of Computer Science, Biomedical and Multimedia Information Technology (BMIT) Group, Madsen Building F09, The University of Sydney, Sydney, NSW 2006, Australia*

[b] *Department of Electronic and Information Engineering, Center for Multimedia Signal Processing (CMSP), Hong Kong Polytechnic University Hung Honi, Kowloan, Hong Kong*

[c] *Department of PET and Nuclear Medicine, Royal Prince Alfred Hospital, Missenden Road, Camperdown, NSW 2050, Australia*

Received 1 July 2000; accepted 9 November 2000

Abstract

The generalized linear least squares (GLLS) algorithm has been found useful in image-wide parameter estimation for the generation of parametric images with positron emission tomography (PET) as it is computationally efficient and statistically reliable. However, the original algorithm was designed for parameter estimation with non-uniformly sampled instantaneous measurements. When dynamic PET data are sampled with the optimal image sampling schedule (OISS) to reduce memory and storage space, only a few temporal image frames are recorded. As a result, the direct application of GLLS is no longer appropriate. In this paper, we extend the GLLS algorithm to a five parameter model for the study of human brain metabolism, which accounts for the effect of cerebral blood volume (CBV), using OISS sampled data, with as few as five temporal samples. The formulation for this new GLLS algorithm is developed, and its computational efficiency and statistical reliability are investigated and validated using computer simulations and clinical PET [18F]-2-fluoro-2-deoxy-D-glucose (FDG) data.

Keywords: Positron emission tomography; Functional imaging; Parameter estimation; Modeling

1. Introduction

Dynamic [18F]-2-fluoro-2-deoxy-D-glucose (FDG) positron emission tomography (PET) is widely used for the measurement of the local cerebral metabolic rate of glucose (LCMRGlc) in the human brain [5,13]. By parameter estimation on a pixel-by-pixel basis, LCMRGlc parametric images can be generated to provide insight into underlying processes and aid diagnosis of the patient's physical condition and the location of cerebral abnormalities. A number of parametric

* Corresponding author. Tel.: +61-2-93512103; fax: +61-2-93513838.

E-mail address: feng@cs.usyd.edu.au (D. Feng).

0169-2607/02/$ - see front matter
PII: S0169-2607(01)00160-2

imaging algorithms have been described previously [1,13,16–18], but most involve certain strong assumptions or require considerable computational time.

The generalized linear least squares (GLLS) algorithm has been shown to offer some advantages over other methods for parameter estimation in non-uniformly sampled biomedical systems. In previous work [7] we found that, compared with existing algorithms [1,13,16–18], the GLLS algorithm: (1) can directly estimate continuous model parameters; (2) does not require initial parameter values; (3) is generally applicable to a variety of models with different structures; (4) can estimate individual model parameters as well as physiological parameters; (5) requires very little computing time; and (6) can produce unbiased estimates [7]. Therefore, this algorithm may be useful in a broad range of parametric imaging applications [2,5,10].

The original GLLS algorithm was developed for a typical conventional sampling schedule (CSS) involving twenty or more dynamic image frames with a standard four-parameter FDG model [7]. An optimal image sampling schedule (OISS) with a much smaller number of image frames (e.g. only four frames) has been previously derived and investigated by computer simulations and clinical studies [12,15]. These previous studies showed that OISS could greatly reduce storage requirements without sacrificing the accuracy of model parameter estimates. More recently it has been shown that the combined application of GLLS and OISS in PET could alleviate two major problems associated with parametric imaging, computational complexity and large image storage requirements [6].

To obtain more accurate and precise parameter estimates, an optimal image sampling schedule for a five-parameter FDG model (OISS5) which includes the cerebral blood volume (CBV) effect has been proposed, in which the effect is modeled by the inclusion of a fifth parameter [4]. We have previously shown [4] that use of OISS5 combined with non-linear least square (NLS) can greatly reduce the number of image frames required and provide comparable metabolic rate estimates (correlation coefficient = 0.995) to those obtainable with CSS in clinical PET studies [4]. However, the feasibility of a five-parameter GLLS algorithm combined with OISS5 (GLLS-OISS5) has not yet been investigated.

The objectives of this paper were:

1. to formulate the theory of generalized linear least squares algorithms for a five-parameter model based on CSS and OISS (CSS5-GLLS and OISS5-GLLS);
2. to validate the statistical reliability and computational efficiency of these algorithms in computer simulation studies at different noise levels; and
3. to compare parameter estimates obtained from OISS5-GLLS with those from (a) non-linear least squares algorithm with CSS5 (CSS5-NLS) and (b) CSS5-GLLS in FDG-PET brain studies.

2. Theory

2.1. The five-parameter FDG model

The four-parameter FDG model is traditionally used to measure the local cerebral metabolic rate of glucose (LCMRGlc) in the human brain following dynamic PET imaging [13],[17]. The mathematical forms describing the four-parameter FDG model are:

$$\begin{cases} \dfrac{\mathrm{d}}{\mathrm{d}t} C_e^*(t) = k_1^* C_p^*(t) - (k_2^* + k_3^*) C_e^*(t) + k_4^* C_m^*(t) \\ \dfrac{\mathrm{d}}{\mathrm{d}t} C_m^*(t) = k_3^* C_e^*(t) - k_4^* C_m^*(t) \end{cases} \tag{1}$$

where $C_p^*(t)$ is the FDG concentration in plasma represented by the plasma time-activity curve (PTAC), $C_e^*(t)$ is the concentration of free FDG in tissue, and $C_m^*(t)$ is the concentration of phosphorylated FDG (FDG-6-PO_4) in tissue. The parameters $k_1^* \sim k_4^*$ are rate constants. The total FDG concentration in tissue $C_i^*(t)$, or tissue time activity concentration curve (TTAC), is given by $C_i^*(t) = C_e^*(t) + C_m^*(t)$.

As this model neglects CBV effect, accounting for the effect of CBV in the FDG model may lead

to more accurate and precise parameter estimates [3,8,14]. Introducing a fifth parameter CBV, the solution of $C_i^*(t)$ for five-parameter model can be defined as [4]

$$C_i^*(t) = (1 - CBV)(C_e^*(t) + C_m^*(t)) + CBV \cdot C_p^*(t) \tag{2}$$

and be further rearranged as

$$C_i^*(t) = \frac{k_1^*(1 - CBV)}{\alpha_2 - \alpha_1}\{(k_3^* + k_4^* - \alpha_1)e^{-\alpha_1 t} + (\alpha_2 - k_3^* - k_4^*)e^{-\alpha_2 t}\} \otimes C_p^*(t) + CBV \cdot C_p^*(t) \tag{3}$$

where $\otimes$ is the convolution operator, and

$$\alpha_{1,2} = (k_2^* + k_3^* + k_4^* \mp \sqrt{(k_2^* + k_3^* + k_4^*)^2 - 4k_2^*k_4^*})/2.$$

LCMRGlc can be calculated from

$$LCMRGlc = (C_p/LC)(k_1^*k_3^*)/(k_2^* + k_3^*) \tag{4}$$

where LC denotes the lumped constant, and C_p is the glucose concentration in plasma.

2.2. Linear least squares (LLS) and GLLS with CSS5 (CSS5-LLS and CSS5-GLLS)

The LLS algorithm is frequently applied to the FDG model to estimate the rate constants from a non-uniformly sampled output function $C_i^*(t)$ [7]. From Eqs. (1) and (2), the input/output dynamics of the model can be described by the following second-order differential equation:

$$\frac{d^2}{dt^2} C_i^*(t) = P_1 \frac{d^2}{dt^2} C_p^*(t) + P_2 \frac{d}{dt} C_p^*(t) + P_3 C_p^*(t) + P_4 \frac{d}{dt} C_i^*(t) + P_5 C_i^*(t) \tag{5}$$

where

$$P_1 = CBV,\ P_2 = (k_2^* + k_3^* + k_4^* - k_1^*) \cdot CBV + k_1^*;$$

$$P_4 = -(k_2^* + k_3^* + k_4^*),\ P_5 = -(k_2^*k_4^*)$$

and

$$P_3 = (k_2^*k_4^* - k_1^*k_3^* - k_1^*k_4^*) \cdot CBV + k_1^*(k_3^* + k_4^*).$$

Integrating Eq. (5) twice from 0 to t, with initial conditions

$$\frac{d}{dt} C_i^*(0^-) = \frac{d}{dt} C_p^*(0^-) = C_i^*(0^-) = C_p^*(0^-) = 0,$$

we obtain a linearized form of the FDG model

$$C_i^*(t) = P_1 C_p^*(t) + P_2 \int_0^t C_p^*(\tau)\, d\tau + P_3 \int_0^t \int_0^\tau C_p^*(s)\, ds\, d\tau + P_4 \int_0^t C_i^*(\tau)\, d\tau + P_5 \int_0^t \int_0^\tau C_i^*(s)\, ds\, d\tau \tag{6}$$

Evaluating $C_i^*(t)$ from Eq. (6) at times t_i defined by CSS5, where $i = 1, 2, \ldots, m$, and adding equation error terms (i.e. the measurement noise), we obtain the following matrix form

$$\mathbf{y} = \mathbf{X}\theta + \varepsilon \tag{7}$$

where $\mathbf{y} = [C_i^*(t_1), C_i^*(t_2), \ldots, C_i^*(t_m)]^{\mathbf{T}}$ are the PET measurements at time $t_1, t_2, \ldots, t_m$, $\mathbf{X}$ is the coefficient matrix,

$$\mathbf{X} = \begin{bmatrix} C_p^*(t_1) & \int_0^{t_1} C_p^*(\tau)\, d\tau & \int_0^{t_1}\int_0^\tau C_p^*(s)\, ds\, d\tau & \int_0^{t_1} C_i^*(\tau)\, d\tau & \int_0^{t_1}\int_0^\tau C_i^*(s)\, ds\, d\tau \\ C_p^*(t_2) & \int_0^{t_2} C_p^*(\tau)\, d\tau & \int_0^{t_2}\int_0^\tau C_p^*(s)\, ds\, d\tau & \int_0^{t_2} C_i^*(\tau)\, d\tau & \int_0^{t_2}\int_0^\tau C_i^*(s)\, ds d\tau \\ \vdots & \vdots & \vdots & \vdots & \vdots \\ C_p^*(t_m) & \int_0^{t_m} C_p^*(\tau)\, d\tau & \int_0^{t_m}\int_0^\tau C_p^*(s)\, ds\, d\tau & \int_0^{t_m} C_i^*(\tau)\, d\tau & \int_0^{t_m}\int_0^\tau C_i^*(s)\, ds d\tau \end{bmatrix}$$

$\theta = [P_1, P_2, P_3, P_4, P_5]^{\mathbf{T}}$ are the macro-parameters to be estimated, and $\varepsilon = [\varepsilon_1, \varepsilon_2, \ldots, \varepsilon_m]^{\mathbf{T}}$ are error terms. Solving Eq. (7) for θ, we obtain the CSS5-LLS estimator of θ,

$$\hat{\theta}_{\text{CSS5-LLS}} = [\mathbf{X}^{\mathbf{T}}\mathbf{X}]^{-1}\mathbf{X}^{\mathbf{T}}\mathbf{y} \tag{8}$$

Once estimates of the macro-parameters are obtained, the micro-parameters, i.e. the rate constants for the FDG model, can be calculated as

$$\hat{k}_1^* = \frac{P_1P_4 + P_2}{1 - P_1},$$

$$\hat{k}_2^* = -\frac{P_1P_5 + P_3}{P_1P_4 + P_2} - P_4,$$

$$\hat{k}_3^* = -(\hat{k}_2^* + \hat{k}_4^* + P_4), \qquad \hat{k}_4^* = -\frac{P_5}{\hat{k}_2^*},$$

$$CBV = P_1 \tag{9}$$

The errors in Eq. (7) are correlated since they are comprised of the direct measurement noise and integrals of the measurement noise. Therefore, the errors in CSS5-LLS are not statistically independent, resulting in biased parameter estimates.

As an alternative, a generalized linear least squares algorithm based on CSS5 (CSS5-GLLS) can be derived. Appendix A gives the mathematical derivation of CSS5-GLLS. The CSS5-GLLS estimator is given by the following matrix equation

$$\hat{\theta}_{\text{CSS5-GLLS}} = [\mathbf{Z}^{\mathbf{T}}\mathbf{Z}]^{-1}\mathbf{Z}^{\mathbf{T}}\mathbf{r} \tag{10}$$

where $\mathbf{r}$ and $\mathbf{Z}$ are given by Eqs. (A7) and (A8) in Appendix A, respectively.

In CSS5-GLLS, an auto-regressive Laplacian filter (see Appendix A) with the previously estimated parameters is defined to whiten the correlated noise and reduce the bias. Eq. (10) can be used repeatedly to refine the estimates of the macro-parameters $\hat{\theta}$ until unbiased estimates are obtained or the termination criterion is reached. Initial values of $\hat{\theta}$ can be obtained from CSS5-LLS. In practice, one or two iterations are sufficient to obtain satisfactory results. No significant improvement was obtained if more iterations were performed. We therefore chose to stop the algorithm after two iterations. The final rate constants are calculated from Eq. (9).

2.3. LLS and GLLS with OISS5 (OISS5-LLS and OISS5-GLLS)

In order to reduce the number of samples and improve the statistical reliability of individual measurements, OISS5 [4] can be combined with the LLS and GLLS methods. However, with OISS5, the duration of sampling intervals is much larger, and the use of instantaneous measurements $C_i^*(t)$ instead of accumulated measurements becomes unrealistic [15]. We therefore modify the linearized form of the five-parameter FDG model (Eq. (6)) using the integral of $C_i^*(t)$ instead of $C_i^*(t)$ itself. Integrating from 0 to time t, we obtain

$$\begin{aligned}
&\int_0^t C_i^*(\tau)\,\mathrm{d}\tau \\
&= P_1\int_0^t C_p^*(\tau)\,\mathrm{d}\tau + P_2\int_0^t\int_0^\tau C_p^*(s)\,\mathrm{d}s\,\mathrm{d}\tau \\
&\quad + P_3\int_0^t\int_0^s\int_0^\tau C_p^*(r)\,\mathrm{d}r\,\mathrm{d}\tau\,\mathrm{d}s \\
&+ P_4\int_0^t\int_0^\tau C_i^*(s)\,\mathrm{d}s\,\mathrm{d}\tau \\
&+ P_5\int_0^t\int_0^s\int_0^\tau C_i^*(r)\,\mathrm{d}r\,\mathrm{d}\tau\,\mathrm{d}s
\end{aligned} \tag{11}$$

Sampling the measurements $\int_0^t C_i^*(\tau)\,\mathrm{d}\tau$ at times corresponding to OISS5 $(\acute{t}_1, \acute{t}_2, \acute{t}_3, \acute{t}_4, \acute{t}_5)$ and adding equation error terms, we obtain

$$\acute{\mathbf{y}} = \acute{\mathbf{X}}\theta + \acute{\varepsilon} \tag{12}$$

where

$$\begin{aligned}
\acute{\mathbf{y}} = \Bigg[&\int_0^{\acute{t}_1} C_i^*(\tau)\,\mathrm{d}\tau, \int_0^{\acute{t}_2} C_i^*(\tau)\,\mathrm{d}\tau, \int_0^{\acute{t}_3} C_i^*(\tau) \\
&\times\,\mathrm{d}\tau, \int_0^{\acute{t}_4} C_i^*(\tau)\,\mathrm{d}\tau, \int_0^{\acute{t}_5} C_i^*(\tau)\,\mathrm{d}\tau\Bigg]^{\mathbf{T}},
\end{aligned}$$

$$\mathbf{X}' = \begin{bmatrix} \int_0^{t_1'} C_p^*(\tau)d\tau & \int_0^{t_1'}\int_0^{\tau} C_p^*(s)dsd\tau & \int_0^{t_1'}\int_0^{s}\int_0^{\tau} C_p^*(r)drd\tau ds & \int_0^{t_1'}\int_0^{\tau} C_i^*(s)dsd\tau & \int_0^{t_1'}\int_0^{s}\int_0^{\tau} C_i^*(r)drd\tau ds \\ \int_0^{t_2'} C_p^*(\tau)d\tau & \int_0^{t_2'}\int_0^{\tau} C_p^*(s)dsd\tau & \int_0^{t_2'}\int_0^{s}\int_0^{\tau} C_p^*(r)drd\tau ds & \int_0^{t_2'}\int_0^{\tau} C_i^*(s)dsd\tau & \int_0^{t_2'}\int_0^{s}\int_0^{\tau} C_i^*(r)drd\tau ds \\ \int_0^{t_3'} C_p^*(\tau)d\tau & \int_0^{t_3'}\int_0^{\tau} C_p^*(s)dsd\tau & \int_0^{t_3'}\int_0^{s}\int_0^{\tau} C_p^*(r)drd\tau ds & \int_0^{t_3'}\int_0^{\tau} C_i^*(s)dsd\tau & \int_0^{t_3'}\int_0^{s}\int_0^{\tau} C_i^*(r)drd\tau ds \\ \int_0^{t_4'} C_p^*(\tau)d\tau & \int_0^{t_4'}\int_0^{\tau} C_p^*(s)dsd\tau & \int_0^{t_4'}\int_0^{s}\int_0^{\tau} C_p^*(r)drd\tau ds & \int_0^{t_4'}\int_0^{\tau} C_i^*(s)dsd\tau & \int_0^{t_4'}\int_0^{s}\int_0^{\tau} C_i^*(r)drd\tau ds \\ \int_0^{t_5'} C_p^*(\tau)d\tau & \int_0^{t_5'}\int_0^{\tau} C_p^*(s)dsd\tau & \int_0^{t_5'}\int_0^{s}\int_0^{\tau} C_p^*(r)drd\tau ds & \int_0^{t_5'}\int_0^{\tau} C_i^*(s)dsd\tau & \int_0^{t_5'}\int_0^{s}\int_0^{\tau} C_i^*(r)drd\tau ds \end{bmatrix}$$

$\theta = [P_1, P_2, P_3, P_4, P_5]^{\mathbf{T}}$, and $\acute{\varepsilon} = [\acute{\varepsilon}_1, \acute{\varepsilon}_2, \acute{\varepsilon}_3, \acute{\varepsilon}_4, \acute{\varepsilon}_5]^{\mathbf{T}}$. Solving Eq. (12), we obtain

$$\hat{\theta}_{\text{OISS5-LLS}} = [\mathbf{X}']^{-1}\mathbf{y}' \tag{13}$$

The rate constants can also be calculated from Eq. (9).

As with CSS5-LLS, estimates obtained from OISS5-LLS contain bias due to the correlation of equation errors which stem from integrations of measurements in $\mathbf{X}'$. The bias in GLLS with OISS5 (OISS5-GLLS) can be reduced using an auto-regressive Laplacian filter. Details on the formulation of OISS5-GLLS are given in Appendix B. The OISS5-GLLS estimator is

$$\hat{\theta}_{\text{OISS5-GLLS}} = [\acute{\mathbf{Z}}]^{-1}\acute{\mathbf{r}} \tag{14}$$

where $\acute{\mathbf{r}}$ and $\acute{\mathbf{Z}}$ are given by Eqs. (B6) and (B7) in Appendix B, respectively.

As with CSS5-GLLS, OISS5-GLLS can be used iteratively to obtain unbiased estimates. However, in practice, a small number of iterations, e.g. one or two, are enough to get unbiased estimates. Therefore, we chose to stop the parameter estimation after two iterations. The rate constants can then be calculated from Eq. (9).

3. FDG studies and data preparation

Dynamic FDG-PET studies were carried out at the National PET/Cyclotron Center, Taipei Veterans General Hospital, Taiwan, using a PC4096-15WB PET scanner (GE/Scanditronix) which has eight detector rings and fifteen slices. This scanner contains 4096 detectors with axial and transaxial resolutions of 6.5 mm full width at half maximum (FWHM). Between 200 and 400 MBq (approximately 0.5 mg) of FDG was injected intravenously and serial arterial blood samples (each 2–3 ml) were taken at 0.25, 0.5, 0.75, 1, 1.25, 1.5, 1.75, 2, 2.5, 3, 3.5, 7, 10, 15, 20, 30, 60, 90 and 120 min post-injection. These samples were immediately placed on ice and the plasma was separated for the determination of plasma FDG and glucose concentrations. PET scanning was performed according to a schedule which consisted of 22 temporal frames: 10×0.2, 2×0.5, 2×1, 1×1.5, 1×3.5, 2×5, 1×10 and 3×30 min scans. The scanning was completed within 120 min of tracer injection. The PET data were corrected for attenuation and decay-corrected to the time of injection and then reconstructed using filtered back-projection with a Hanning filter. The reconstructed images were 128×128 with pixel size of 2 mm^2.

In general, a TTAC curve can be obtained from each pixel. However, many TTAC curves have similar kinetics. A clustering technique [9], was used to group image-wide TTACs according to a similarity criterion. The similarity measure used was the Euclidean distance D between the TTACs with an adaptive threshold $T = C\sigma_{\text{plane}}$, where C is an empirically determined constant (1.5 in this study), and σ_{plane} is the standard deviation of the plane pixel values in the last frame. Here 'plane' stands for a cross-section of the brain, and 'frame' stands for the set of planes acquired at each time point. The standard deviation provides an indication of the overall variability in the pixel TTACs. TTACs with similar kinetics (i.e. $D \leq T$) were classified into the same cluster, and conversely, TTACs with low degrees of similarity (i.e. $D > T$) were placed in

different groups. The pixels belonging to each cluster were then treated as a separate brain region of interest (ROI). TTACs were generated from each of these ROIs for model fitting. Cluster analysis was applied to three clinical FDG-PET studies. Eight clusters were identified in two studies, and seven in one, resulting in a total of 23 ROIs.

4. Simulation study, results and discussion

4.1. Simulation

Computer simulations were performed to assess the statistical reliability and computational efficiency of the GLLS algorithm with CSS5 and OISS5. Averaged parameters [$k_1^* = 0.0315$ ml min^{-1} g^{-1}, $k_2^* = 0.0978$ min^{-1}, $k_3^* = 0.0515$ min^{-1}, $k_4^* = 0.00888$ min^{-1}, CBV = 4.425 ml 100 g^{-1}] derived from four sets of typical micro-parameters of the FDG models obtained in human study [8], were used as model parameters in the simulations. Estimation of $k_1^* \sim k_4^*$, the CBV and the combined parameter $K = (k_1^* k_3^*)/(k_2^* + k_3^*)$ are our primary interest in this study. The plasma time activity curve from a clinical FDG study was used as the input function $C_p^*(t)$. PET measurements $C_i^*(t)$were simulated according to Eq. (3) with the above parameter values for two sampling schedules: CSS5 and OISS5. A 60- and 120-min PET scanning were used in our simulation study. For the 60-min PET scans, sampling times with CSS5 were 0.16, 0.33, 0.49, 0.66, 0.82, 1.0, 1.5, 2.0, 2.5, 3.0, 5.0, 10.0, 15.0, 20.0, 25.0, 30.0, 35.0, 40.0, 45.0, 50.0, 55.0 and 60.0 min, while those with OISS5 were 0.683, 2.950, 12.40, 40.917, 60.0 min. For the 120-min PET scans, sampling times with CSS5 were 0.2, 0.4, 0.6, 0.8, 1.0, 1.2, 1.4, 1.6, 1.8, 2.0, 2.5, 3.0, 4.0, 5.0, 6.5, 10.0, 15.0, 20.0, 30.0, 60.0, 90.0 and 120.0 min, while those with OISS5 were 0.717, 3.20, 14.450, 75.383 and 120.0 min [4].

Since PET measurements depend on count rate and scan duration, the variance structure of the measurement error can be described as

$$\sigma^2(\dot{t}_k) = \alpha \times C_i^*(\dot{t}_k)/\Delta t_k, \quad (15)$$

where $\sigma^2(\dot{t}_k)$ is the variance of the output function measurement at the mid-time $\dot{t}_k$ of the kth scanning interval, $\Delta t_k = t_k - t_{k-1}$, and α is a proportionality constant that determines the noise level in the measurement. A pseudo-random number generator was used to generate the Gaussian noise added to the PET measurements, $C_i^*(t)$, according to the error variance from Eq. (15), in which α was set to 0.0 (noise free), 0.1, 0.2, 0.5, 1.0, 2.0 and 4.0, respectively.

The standard deviation (S.D.) and mean were obtained from 100 Monte-Carlo simulation runs at each noise level. Only one run was performed for the noise free case. The statistical properties of four different models, CSS5-LLS, CSS5-GLLS, OISS5-LLS and OISS5-GLLS, were compared with those of NLS with CSS5 (CSS5-NLS), which was treated as the gold standard.

In OISS5-LLS, the numerical integration of accumulated measurements requires care. Since the number of samples is greatly reduced, and the sampling intervals are much longer, the use of trapezoidal integration which has only first-order algebraic accuracy (the straight line) may lead to numerical integration errors and error propagation in the parameter estimates. To overcome this, the weighted parabola overlapping (WPO) method [19] which has third-order algebraic accuracy was used (see Appendix C).

4.2. Results and discussion

Fig. 1 illustrates the mean and standard deviation of the estimated parameters k_1, k_2, k_3, k_4, CBV, and the combined parameter K obtained from the simulation study with 120-min scan duration for seven different noise levels. The 'T' bars indicate the S.D. and the dotted lines depict the actual parameter values. For those estimated parameters obtained from the simulation study with 60-min scan duration, the means and S.D. are shown in Fig. 2. We can easily see that for noise free data (e.g. noise level is 0.0), compared with the CSS5-NLS, the parameters k_1, k_2, k_3, k_4, CBV, and K estimated by CSS5-GLLS and OISS5-GLLS were significantly improved compared with those estimated by CSS5-LLS and OISS5-LLS, for both scan duration. In other

words, CSS5-GLLS and OISS5-GLLS provided lower bias than CSS5-LLS and OISS5-LLS. The results obtained at different noise levels also show that CSS5-GLLS and OISS5-GLLS provided better estimates than CSS5-LLS and OISS5-LLS that were consistent with CSS5-NLS. The S.D. indi-

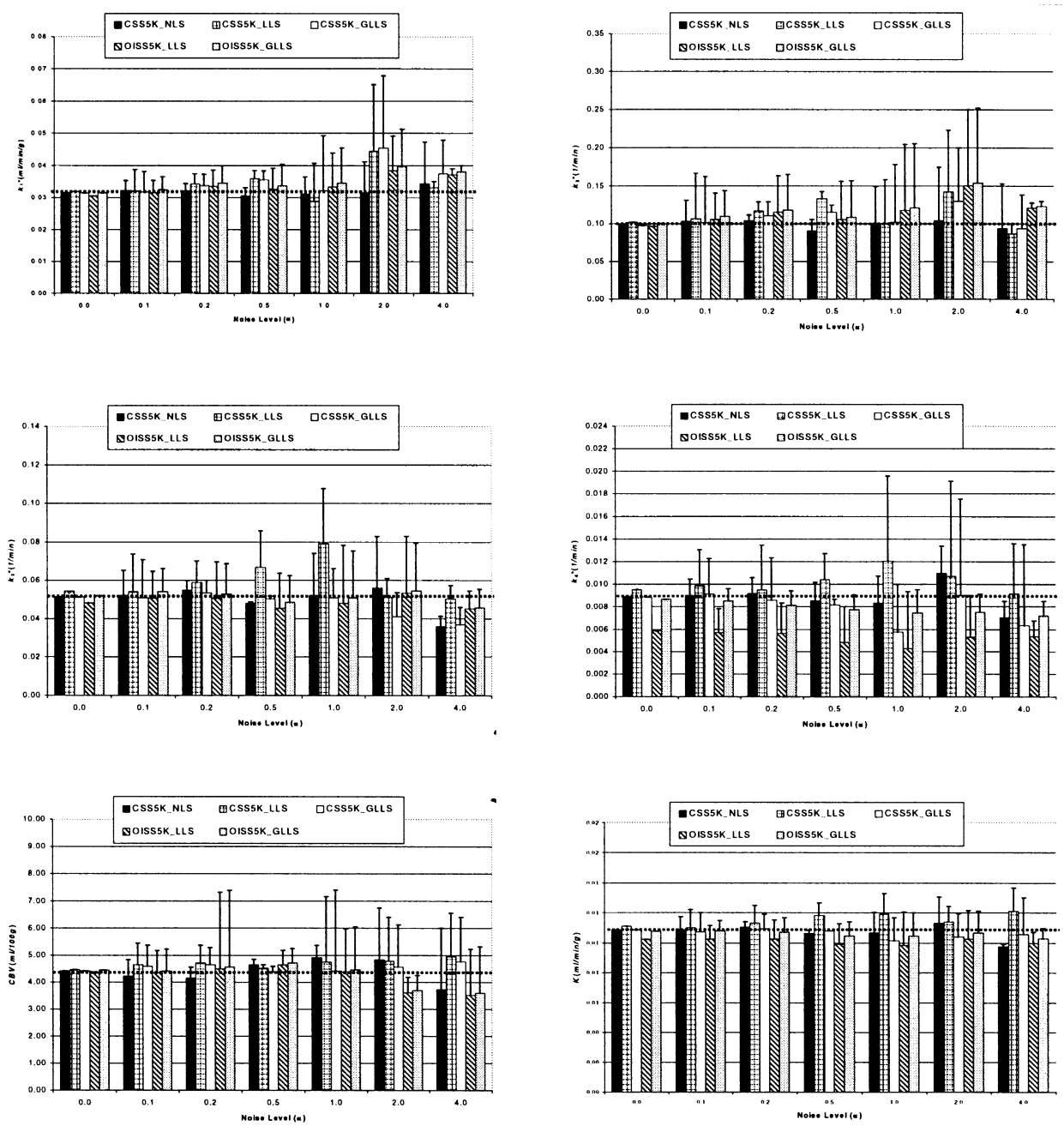

Fig. 1. Plots of the estimated parameter means vs. noise levels. The estimated means k_1, k_2, k_3, k_4, CBV, and the combined parameter K are obtained from the simulation study with 120-min scan duration. The 'T' bars indicate the standard deviation (S.D.) and the dotted lines depict the actual parameter values.

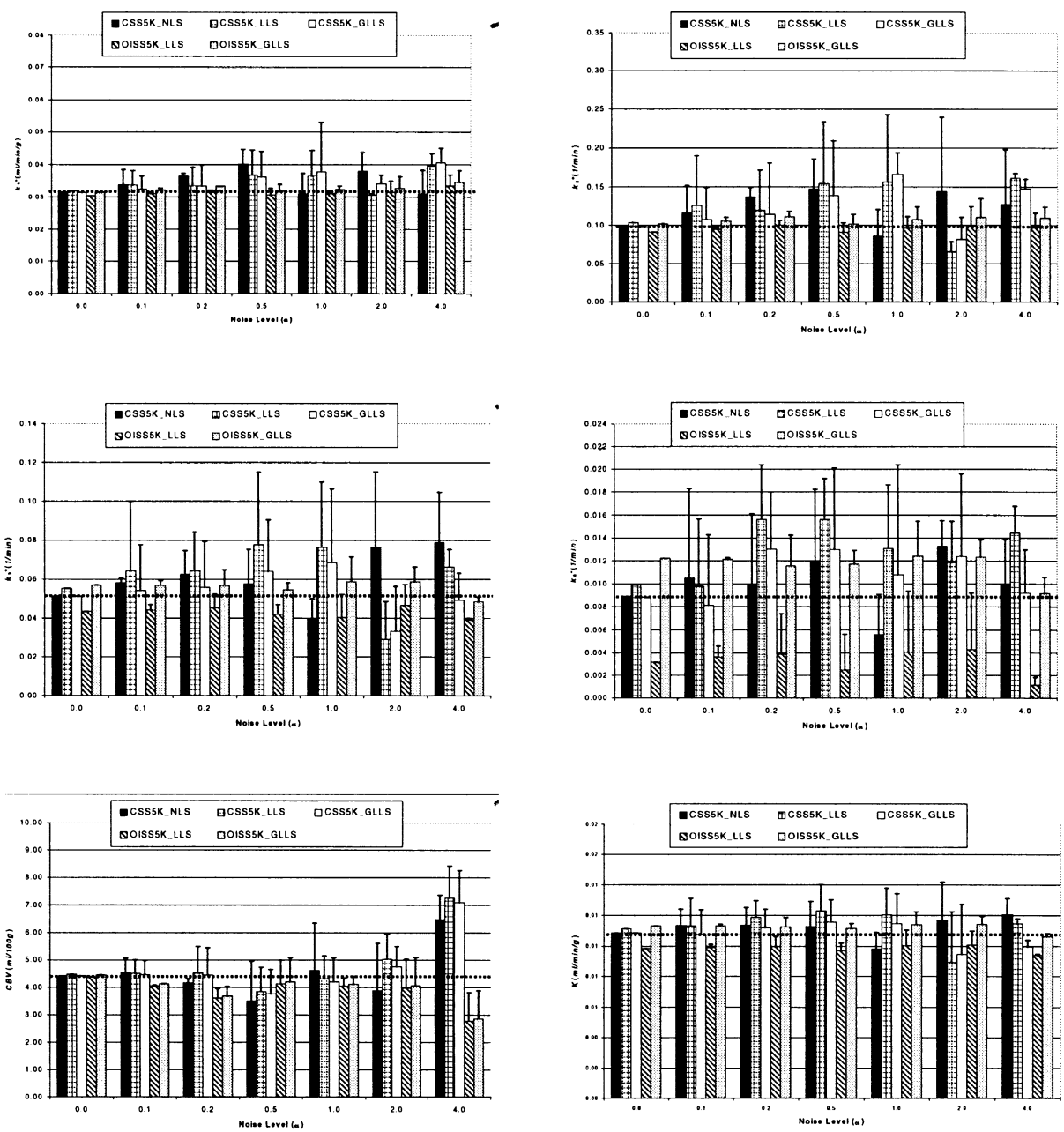

Fig. 2. Plots of the estimated parameter means vs. noise levels. The estimated means k_1, k_2, k_3, k_4, CBV, and the combined parameter K are obtained from the simulation study with 60-min scan duration. The 'T' bars indicate the standard deviation (S.D.) and the dotted lines depict the actual parameter values.

cate that CSS5-NLS, CSS5-GLLS, and OISS5-GLLS provided estimates with similar statistical reliability. Note that our primary interest is to estimate the combined parameter K or, equivalently, the regional LCMRGlc. The statistical results given in Figs. 1 and 2 show that the mean

estimated values of K for CSS5-NLS, CSS5-GLLS and OISS5-GLLS are quite similar. All of the results with the simulation study demonstrate that OISS5-GLLS provides estimates in good agreement with CSS5-NLS and CSS5-GLLS.

Two iterations of CSS5-GLLS and OISS5-GLLS removed the bias in CSS5-LLS and OISS5-LLS, demonstrating that less-biased estimates can be obtained in the absence of noise using CSS5-GLLS. For OISS5-GLLS, however, the estimates were still somewhat biased after two iterations. When further iterations were employed, we found the estimation accuracy was further improved. However, our simulations showed only small improvement after the first few iterations, and the use of more than five iterations is probably not justified. We found that 10–20 iterations for CSS5-NLS and two iterations for OISS5-GLLS were sufficient. The average run time for 100 simulation runs with noise level 4.0, $T_{\text{CSS5-NLS}}$, was 33.6 s and $T_{\text{OISS5-GLLS}}$ was 0.63 s. OISS5-GLLS therefore provides a significant improvement in computational efficiency. Since OISS5 requires only five scanning intervals while CSS5-NLS requires twenty-two, OISS5-GLLS can not only provide accurate and reliable parameter estimates, but also greatly reduce image storage requirements.

5. Clinical studies, results and discussion

5.1. The clinical studies

OISS5-GLLS parameter estimates were compared with those of CSS5-NLS and CSS5-GLLS in 23 ROIs obtained from three dynamic FDG-PET brain studies. Since the clinical data were acquired with a conventional sampling schedule, TTACs for CSS5 were obtained directly from the clinical data. TTACs for OISS5 were obtained by a re-sampling technique which combines and interpolates the measured CSS temporal frames according to the OISS5 scanning intervals derived previously [4,11]. Model parameters were estimated for the 23 ROIs using CSS5-NLS, CSS5-GLLS, and OISS5-GLLS. These parameters were then used to calculate LCMRGlc using Eq. (4), and the results were compared via linear regression analysis and paired Student's t-test. The

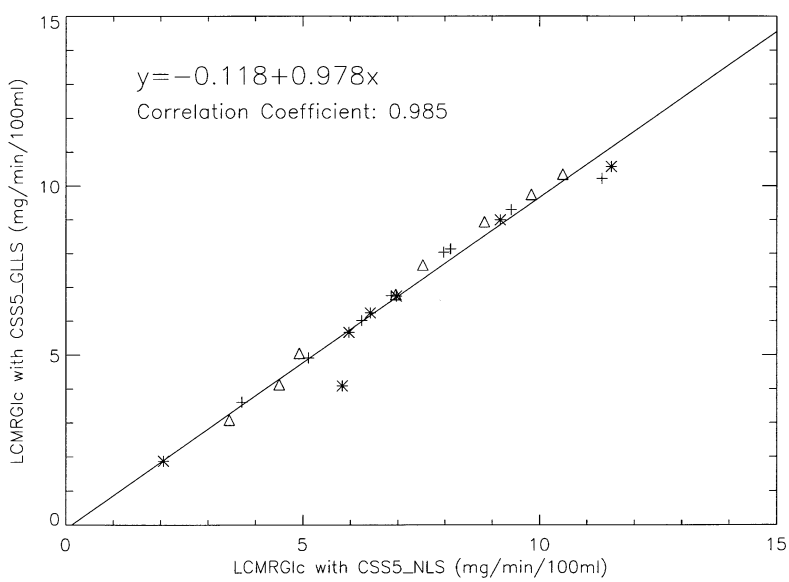

Fig. 3. Correlation of LCMRGlc estimated by the nonlinear least squares (NLS) and generalized linear least square (GLLS) method with a conventional sampling schedule and the five-parameter FDG model (CSS5). The plus, asterisk and triangle symbols represent mean results for three different FDG-PET studies.

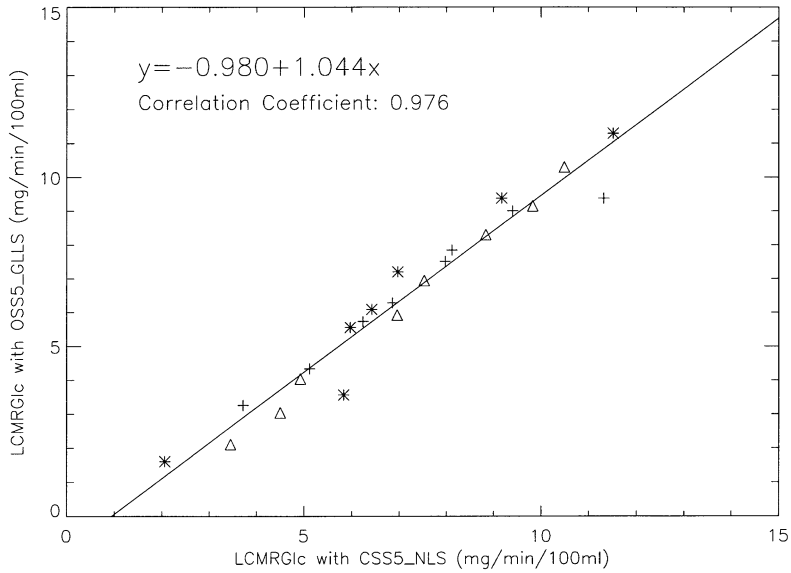

Fig. 4. Correlation of LCMRGlc estimated by the nonlinear least squares (NLS) with CSS5 and generalized linear least square (GLLS) method with the optimal image sampling schedule and the five-parameter FDG model (OISS5). The plus, asterisk and triangle symbols represent mean results for three different FDG-PET studies.

lumped constant (LC) for this clinical study was calculated to be 0.307248 using the method described in [13], and the glucose concentration in plasma (C_p) to 1.25.

5.2. Results and discussion

The correlations in LCMRGlc estimates between CSS5-NLS and each of CSS5-GLLS and OISS5-GLLS are shown in Figs. 3 and 4. For CSS5-GLLS, the correlation coefficient was $r = 0.985$ with a correlation line: $y = -0.118 + 0.978x$. Similar results were obtained for OISS5-GLLS: $y = -0.980 + 1.044x$ and $r = 0.976$. In addition, paired Student's t-test was performed on LCMRGlc estimates. For CSS5-NLS versus CSS5-GLLS, the t-value was 0.373 with $P = 0.711$; and for CSS5-NLS versus OISS5-GLLS, the t-value was 0.866 and $P = 0.391$. These results demonstrate that LCMRGlc estimates obtained by OISS5-GLLS are not significantly different from those from CSS5-NLS and CSS5-GLLS in terms of the accuracy and precision of the estimated parameters.

6. Summary

We have presented GLLS algorithms for a five-parameter FDG model, in which the effect of CBV has been taken into account. These algorithms can be applied to data acquired with both conventional and optimal image sampling schedules. The statistical reliability and computational efficiency of the algorithms have been investigated using computer simulations and clinical FDG-PET studies. The results show that compared with CSS5-NLS and CSS5-GLLS, the OISS5-GLLS algorithm provides similar parameter estimates in dynamic FDG-PET studies, while significantly reducing computational complexity and image storage requirements. This algorithm is therefore potentially very useful in image wide parameter estimation for the generation of functional images in dynamic PET studies.

Acknowledgements

This research is supported by the ARC and RGC Grants. The authors are grateful to the

National PET/Cyclotron Center, Taipei Veterans General Hospital Taiwan for their kind assistance.

Appendix A

The CSS5-GLLS can be derived from the second-order differential equation (Eq. (5)). Taking the Laplace transform of Eq. (5), we have

$$s^2C_i^*[s] = s^2P_1C_p^*[s] + sP_2C_p^*[s] + P_3C_p^*[s] + sP_4C_i^*[s] + P_5C_i^*[s] \quad \text{(A1)}$$

where initial conditions are assumed to be zero. Rearranging and adding a white (uncorrelated) Laplacian noise term $E[s]$, we have

$$C_i^*[s] = \frac{s^2P_1C_p^*[s] + sP_2C_p^*[s] + P_3C_p^*[s]}{s^2 - sP_4 - P_5} + E[s] \quad \text{(A2)}$$

Eq. (A2) can then be rearranged as

$$s^2C_i^*[s] = s^2P_1C_p^*[s] + sP_2C_p^*[s] + P_3C_p^*[s] + sP_4C_i^*[s] + P_5C_i^*[s] + (s^2 - sP_4 - P_5)E[s] \quad \text{(A3)}$$

The noise term $(s^2 - sP_4 - P_5)E[s]$ is coloured (correlated) noise, even though the direct measurement noise $E[s]$ is white. We can define an auto-regressive filter to whiten the coloured noise term and reduce the bias. Once rough estimates of the parameters $\hat{P}_1 \sim \hat{P}_5$ are obtained, the filter $F_{CSS5}[s] = s^2 - s\hat{P}_4 - \hat{P}_5$ is defined. Dividing Eq. (A3) by this filter, we get

$$\frac{s^2C_i^*[s]}{s^2 - s\hat{P}_4 - \hat{P}_5} = \frac{s^2P_1C_p^*[s]}{s^2 - s\hat{P}_4 - \hat{P}_5} + \frac{sP_2C_p^*[s]}{s^2 - s\hat{P}_4 - \hat{P}_5} + \frac{P_3C_p^*[s]}{s^2 - s\hat{P}_4 - \hat{P}_5} + \frac{sP_4C_i^*[s]}{s^2 - s\hat{P}_4 - \hat{P}_5} + \frac{P_5C_i^*[s]}{s^2 - s\hat{P}_4 - \hat{P}_5} + \frac{s^2 - sP_4 - P_5}{s^2 - s\hat{P}_4 - \hat{P}_5}E[s] \quad \text{(A4)}$$

As $(s^2 - sP_4 - P_5) \approx (s^2 - s\hat{P}_4 - \hat{P}_5)$, the coloured noise is whitened and when $(s^2 - sP_4 - P_5) = (s^2 - s\hat{P}_4 - \hat{P}_5)$, the estimates obtained from Eq. (A4) are unbiased. Rearranging and taking the inverse Laplace transform of Eq. (A4), we have

$$\begin{aligned} &C_i^*(t) + \hat{P}_4\psi_1 \otimes C_i^*(t) + \hat{P}_5\psi_2 \otimes C_i^*(t) \\ &= P_1(C_p^*(t) + \hat{P}_4\psi_1 \otimes C_p^*(t) + \hat{P}_5\psi_2 \otimes C_p^*(t)) \\ &+ P_2\psi_1 \otimes C_p^*(t) + P_3\psi_2 \otimes C_p^*(t) + P_4\psi_1 \otimes C_i^*(t) \\ &+ P_5\psi_2 \otimes C_i^*(t) \end{aligned} \quad \text{(A5)}$$

where,

$$\psi_1(t) = \frac{1}{\lambda_2 - \lambda_1}\{\lambda_2 e^{-\lambda_2 t} - \lambda_1 e^{-\lambda_1 t}\},$$

$$\psi_2(t) = \frac{1}{\lambda_2 - \lambda_1}\{e^{-\lambda_1 t} - e^{-\lambda_2 t}\}$$

and

$$\lambda_{1,2} = -(\hat{P}_4 \pm \sqrt{\hat{P}_4^2 + 4\hat{P}_5})/2.$$

For simplicity, the filtered noise term $(s^2 - sP_4 - P_5)/(s^2 - s\hat{P}_4 - \hat{P}_5)E[s]$ is not re-written in Eq. (A5). Based on CSS5, sampling Eq. (A5) at time $t_1, t_2, \ldots, t_m$, we obtain

$$\mathbf{r} = \mathbf{Z}\theta \quad \text{(A6)}$$

where

$$\mathbf{r} = \begin{bmatrix} C_i^*(t_1) + \hat{P}_4\psi_1 \otimes C_i^*(t_1) + \hat{P}_5\psi_2 \otimes C_i^*(t_1) \\ C_i^*(t_2) + \hat{P}_4\psi_1 \otimes C_i^*(t_2) + \hat{P}_5\psi_2 \otimes C_i^*(t_2) \\ \vdots \\ C_i^*(t_m) + \hat{P}_4\psi_1 \otimes C_i^*(t_m) + \hat{P}_5\psi_2 \otimes C_i^*(t_m) \end{bmatrix} \quad \text{(A7)}$$

$$\begin{aligned} \mathbf{Z} = \Bigg[& C_p^*(t_1) + \hat{P}_4\psi_1 \otimes C_p^*(t_1) + \\ & \hat{P}_5\psi_2 \otimes C_p^*(t_1)\psi_1 \otimes C_p^*(t_1)\psi_2 \otimes C_p^*(t_1)\psi_1 \otimes C_i^*(t_1)\psi_2 \\ & \otimes C_i^*(t_1)C_p^*(t_2) + \hat{P}_4\psi_1 \otimes C_p^*(t_2) + \hat{P}_5\psi_2 \\ & \otimes C_p^*(t_2)\psi_1 \otimes C_p^*(t_2)\psi_2 \otimes C_p^*(t_2)\psi_1 \otimes C_i^*(t_2)\psi_2 \\ & \otimes C_i^*(t_2)\cdots\cdots C_p^*(t_m) + \hat{P}_4\psi_1 \otimes C_p^*(t_m) + \hat{P}_5\psi_2 \\ & \otimes C_p^*(t_m)\psi_1 \otimes C_p^*(t_m)\psi_2 \otimes C_p^*(t_m)\psi_1 \otimes C_i^*(t_m)\psi_2 \\ & \otimes C_i^*(t_m) \Bigg] \end{aligned} \quad \text{(A8)}$$

and $\theta = [P_1, P_2, P_3, P_4, P_5]^{\mathrm{T}}$.

Solving Eq. (A6) for θ, we obtain the CSS5-GLLS estimator

$$\hat{\theta}_{\text{CSS5-GLLS}} = [\mathbf{Z}^{\mathbf{T}}\mathbf{Z}]^{-1}\mathbf{Z}^{\mathbf{T}}\mathbf{r} \tag{A9}$$

Appendix B

The OISS5-GLLS can also be derived from Eq. (5). Rearranging the Laplace transform of Eq. (5) and adding a white Laplacian noise term $E[s]$, it becomes

$$\frac{1}{s}C_i^*[s] = \frac{s^2P_1C_p^*[s] + sP_2C_p^*[s] + P_3C_p^*[s]}{s(s^2 - sP_4 - P_5)} + E[s] \tag{B1}$$

Rearranging Eq. (B1), we obtain

$$\begin{aligned} s^2C_i^*[s] = {} & s^2P_1C_p^*[s] + sP_2C_p^*[s] + P_3C_p^*[s] \\ & + sP_4C_i^*[s] + P_5C_i^*[s] \\ & + s(s^2 - sP_4 - P_5)E[s] \end{aligned} \tag{B2}$$

An auto-regressive filter $F_{\text{OISS5}}[s] = s(s^2 - s\hat{P}_4 - \hat{P}_5)$ is defined to whiten the coloured noise $s(s^2 - sP_4 - P_5)E[s]$, where $\hat{P}_4$,$\hat{P}_5$ are the rough estimates of the macro-parameters. Dividing Eq. (B2) by the filter $F_{\text{OISS5}}[s]$, we obtain

$$\begin{aligned} \frac{s^2C_i^*[s]}{s^2 - s\hat{P}_4 - \hat{P}_5} = {} & \frac{s^2P_1C_p^*[s]}{s^2 - s\hat{P}_4 - \hat{P}_5} + \frac{sP_2C_p^*[s]}{s^2 - s\hat{P}_4 - \hat{P}_5} \\ & + \frac{P_3C_p^*[s]}{s^2 - s\hat{P}_4 - \hat{P}_5} \\ & + \frac{P_4C_i^*[s]}{s^2 - s\hat{P}_4 - \hat{P}_5} + \frac{P_5C_i^*[s]}{s(s^2 - s\hat{P}_4 - \hat{P}_5)} \\ & + \frac{s(s^2 - sP_4 - P_5)}{s(s^2 - s\hat{P}_4 - \hat{P}_5)}E[s] \end{aligned} \tag{B3}$$

Discarding the filtered noise term

$$\frac{s(s^2 - sP_4 - P_5)}{s(s^2 - s\hat{P}_4 - \hat{P}_5)}E[s]$$

from Eq. (B3) and taking the inverse Laplace transform of Eq. (B3), we have

$$\begin{aligned} & \psi_1 \otimes C_i^*(t) \\ & = P_1\psi_1 \otimes C_p^*(t) + P_2\psi_2 \otimes C_p^*(t) \\ & \quad + P_3\left\{\frac{1}{\lambda_1\lambda_2}\int_0^t C_p^*(\tau)\,\mathrm{d}\tau + \psi_3 \otimes C_p^*(t)\right\} \\ & \quad + P_4\psi_2 \otimes C_i^*(t) \\ & \quad + P_5\left\{\frac{1}{\lambda_1\lambda_2}\int_0^t C_i^*(\tau)\,\mathrm{d}\tau + \psi_3 \otimes C_i^*(t)\right\} \end{aligned} \tag{B4}$$

where

$$\begin{aligned} & \psi_1(t) = \frac{1}{\lambda_2 - \lambda_1}\{\lambda_2 e^{-\lambda_2 t} - \lambda_1 e^{-\lambda_1 t}\},\ \psi_2(t) \\ & \qquad = \frac{1}{\lambda_2 - \lambda_1}\{e^{-\lambda_1 t} - e^{-\lambda_2 t}\} \\ & \psi_3(t) = \frac{1}{\lambda_2 - \lambda_1}\left\{\frac{1}{\lambda_2}e^{-\lambda_2 t} - \frac{1}{\lambda_1}e^{-\lambda_1 t}\right\}, \quad \text{and} \\ & \lambda_{1,2} = -\frac{\hat{P}_4 \pm \sqrt{\hat{P}_4^2 + 4\hat{P}_5}}{2}. \end{aligned}$$

Based on OISS5, digitizing Eq. (B4) by taking measurements at optimally sampled time t_1, t_2, t_3, t_4, t_5, we obtain the following matrix form

$$\mathbf{r}' = \mathbf{Z}'\theta \tag{B5}$$

where

$$\begin{aligned} \mathbf{r}' = {} & [\psi_1 \otimes C_i^*(t_1), \psi_1 \otimes C_i^*(t_2), \psi_1 \otimes C_i^*(t_3), \psi_1 \\ & \otimes C_i^*(t_4), \psi_1 \otimes C_i^*(t_5)]^{\mathbf{T}} \end{aligned} \tag{B6}$$

$$\mathbf{Z}' = \begin{bmatrix} \psi_1 \otimes C_p^*(t_1') & \psi_2 \otimes C_p^*(t_1') & \frac{1}{\lambda_1\lambda_2}\int_0^{t_1'} C_p^*(\tau)d\tau + \psi_3 \otimes C_p^*(t_1') & \psi_2 \otimes C_i^*(t_1') & \frac{1}{\lambda_1\lambda_2}\int_0^{t_1'} C_i^*(\tau)d\tau + \psi_3 \otimes C_i^*(t_1') \\ \psi_1 \otimes C_p^*(t_2') & \psi_2 \otimes C_p^*(t_2') & \frac{1}{\lambda_1\lambda_2}\int_0^{t_2'} C_p^*(\tau)d\tau + \psi_3 \otimes C_p^*(t_2') & \psi_2 \otimes C_i^*(t_2') & \frac{1}{\lambda_1\lambda_2}\int_0^{t_2'} C_i^*(\tau)d\tau + \psi_3 \otimes C_i^*(t_2') \\ \psi_1 \otimes C_p^*(t_3') & \psi_2 \otimes C_p^*(t_3') & \frac{1}{\lambda_1\lambda_2}\int_0^{t_3'} C_p^*(\tau)d\tau + \psi_3 \otimes C_p^*(t_3') & \psi_2 \otimes C_i^*(t_3') & \frac{1}{\lambda_1\lambda_2}\int_0^{t_3'} C_i^*(\tau)d\tau + \psi_3 \otimes C_i^*(t_3') \\ \psi_1 \otimes C_p^*(t_4') & \psi_2 \otimes C_p^*(t_4') & \frac{1}{\lambda_1\lambda_2}\int_0^{t_4'} C_p^*(\tau)d\tau + \psi_3 \otimes C_p^*(t_4') & \psi_2 \otimes C_i^*(t_4') & \frac{1}{\lambda_1\lambda_2}\int_0^{t_4'} C_i^*(\tau)d\tau + \psi_3 \otimes C_i^*(t_4') \\ \psi_1 \otimes C_p^*(t_5') & \psi_2 \otimes C_p^*(t_5') & \frac{1}{\lambda_1\lambda_2}\int_0^{t_5'} C_p^*(\tau)d\tau + \psi_3 \otimes C_p^*(t_5') & \psi_2 \otimes C_i^*(t_5') & \frac{1}{\lambda_1\lambda_2}\int_0^{t_5'} C_i^*(\tau)d\tau + \psi_3 \otimes C_i^*(t_5') \end{bmatrix} \tag{B7}$$

and $\theta = [P_1, P_2, P_3, P_4, P_5]^{\mathbf{T}}$. Solving Eq. (B5) for θ, we obtain the OISS5-GLLS estimator

$$\hat{\theta}_{\text{OISS5-GLLS}} = [\acute{\mathbf{Z}}]^{-1}\acute{\mathbf{r}} \tag{B8}$$

Appendix C

The weighted parabola overlapping (WPO) technique has been previously investigated [19]. This method guarantees integral values of function $f(t)$ within the interval t_i to t_{i+1}, to third-order algebraic accuracy. WPO is based on two weighted integral values obtained from overlapping parabola functions defined at four points t_{i-1}, t_i, t_{i+1} and t_{i+2}. In [19], the following equations were derived for WPO,

$$\begin{aligned}
S_i &= (1-\alpha_i)S_i^b + \alpha_i S_{i+1}^f \\
\alpha_i &= (t_{i+1} + t_i - 2t_i)/[2(t_{i+2} - t_{i-1})] \\
S_i^b &= (t_{i+1} - t_i)[(f_i + f_{i+1})/2 + P_i/Q_i] \\
S_i^f &= (t_i - t_{i-1})[(f_i + f_{i-1})/2 + P_i Q_i] \\
P_i &= f_i - [(t_{i+1} - t_i)f_{i-1} + (t_i - t_{i-1})f_{i+1}] \\
&\quad \times /(t_{i+1} - t_{i-1})/6 \\
Q_i &= (t_i - t_{i-1})/(t_{i+1} - t_i)
\end{aligned} \tag{C1}$$

The integral value S_i in Eq. (C1) obtains third-order algebraic accuracy by weighting and overlapping backward value S_i^b and forward value S_i^f using the weighting coefficient α_i. Therefore, we can obtain approximate integral values of third-order algebraic accuracy during every interval except during the first, t_0 and t_1, and the last, t_{m-1} and t_m, intervals. If we require integral values in these intervals to possess third-order algebraic accuracy, Lagrange interpolation can be used. However, if only second-order algebraic accuracy in these intervals is required, we can assign values $\alpha_0 = 1$ and $\alpha_{m-1} = 0$ in Eq. (C1).

References

[1] R.E. Carson, S.C. Huang, M.E. Green, Weighted integration method for local cerebral blood flow measurements with positron emission tomography, J. Cereb. Blood Flow Metab. 6 (1986) 245–258.

[2] K. Chen, M. Lawson, E. Reiman, D. Feng, S.C. Huang, D. Bandy, D. Ho, L. Yun, A. Palant, Generalized linear least square method for fast generation of myocardial blood flow parametric images with N-13 Ammonia PET, IEEE Trans. Med. Imag. 17 (2) (1998) 236–243.

[3] A.C. Evans, M. Diksic, Y.L. Yamamoto, A. Kato, A. Dagher, C. Redies, A. Hakim, Effect of vascular activity in the determination of rate constants for the uptake of 18F-labeled 2-fluoro-2-deoxy-D-glucose: error analysis and normal values in older subjects, J. Cereb. Blood Flow Metab. 6 (1986) 724–738.

[4] D. Feng, W. Cai, R. Fulton, An optimal image sampling schedule design for cerebral blood volume and partial volume correction in neurologic FDG-PET studies, Austr. N.Z. J. Med. 28 (3) (1998) 361.

[5] D. Feng, D. Ho, K. Chen, L.C. Wu, J.K. Wang, R.S. Liu, S.H. Yeh, An evaluation of the algorithms for determining local cerebral metabolic rates of glucose using positron emission tomography dynamic data, IEEE Trans. Med. Imag. 14 (1995) 697–710.

[6] D. Feng, D. Ho, K.K. Lau, W.C. Siu, GLLS for optimally sampled continuous dynmaic system modeling: theory and algorithm, in: R.E. Carson, et al. (Eds.), Quantitative Functional Brain Imaging with Positron Emission Tomography, Academic Press, San Diego, 1960, pp. 339–345.

[7] D. Feng, S.C. Huang, Z. Wang, D. Ho, An unbiased parametric imaging algorithm for non-uniformly sampled biomedical system parameter estimation, IEEE Trans. Med. Imag. 15 (1996) 512–518.

[8] R.A. Hawkins, M.E. Phelps, S.C. Huang, Effects of temporal sampling, glucose metabolic rates, and disruptions of the blood-brain barrier on the FDG model with and without a vascular compartment: studies in human brain tumours with PET, J. Cereb. Blood Flow Metab. 6 (1986) 170–183.

[9] D. Ho, D. Feng, K. Chen, Dynamic image data compression in spatial and temporal domains: theory and algorithm, IEEE Trans. Info. Tech. Biomed. 1 (4) (1997) 219–228.

[10] D. Ho, D. Feng, K. Chen, A new method for the analysis of multiple positron emission tomography dynamic datasets: an example applied to the estimation of the cerebral metabolic rate of oxygen, Med. Biol. Eng. Comput. 36 (1) (1998) 83–90.

[11] D. Ho, D. Feng, L.C. Wu, An assessment of optimal image sampling schedule design in dynamic PET-FDG studies, in: R.E. Carson, et al. (Eds.), Quantitative Functional Brain Imaging with Positron Emission Tomography, Academic Press, San Diego, 1998, pp. 315–320.

[12] K. Ho-Shon, D. Feng, R.A. Hawkins, S. Meikle, M. Fulham, X. Li, Optimised sampling and parameter estimation for quantification in whole body PET, IEEE Trans. Biomed. Eng. 43 (1996) 1021–1028.

[13] S.C. Huang, M.E. Phelps, E.J. Hoffman, K. Sideris, C.J. Selin, D.E. Kuhl, Non-invasive determination of local cerebral metabolic rate of glucose in man, Am. J. Physiol. 238 (1980) E69–E82.

[14] A. Kato, M. Diksic, Y.L. Yamamoto, S.C. Strother, W. Feindel, An improved approach for measurement of regional cerebral rate constants in the deoxyglucose method with positron emission tomography, J. Cereb. Blood Flow Metab. 4 (1984) 555–563.

[15] X. Li, D. Feng, K. Chen, Optimal image sampling schedule: a new effective way to reduce dynamic image storage space and functional image processing time, IEEE Trans. Med. Imag. 15 (1996) 710–719.

[16] C.S. Patlak, R.G. Blasberg, J. Fenstermacher, Graphical evaluation of blood to brain transfer constants from multiple-time uptake data, J. Cereb. Blood Flow Metab. 3 (1983) 1–7.

[17] M.E. Phelps, S.C. Huang, E.J. Hoffman, C. Selin, L. Sokoloff, D.E. Kuhl, Tomographic measurement of local cerebral glucose metabolic rate in humans with FDG: validation of method, Ann. Neurol. 6 (1979) 371–388.

[18] M.E. Phelps, J. Mazziotta, H. Schelbert, Positron Emission Tomography and Autoradiography: Principles and Applications for the Brain and Heart, Raven Press, New York, 1986.

[19] Z. Wang, D. Feng, Continuous-time system modelling using the weighted-parabola-overlapping numerical integration method, Int. Sys. Sci. 23 (1992) 1361–1369.